









Effects of LED Device Size on UV-C Short-Range LoS Optical Wireless Communication

Jordan Hill , Cheng Chen , Enyuan Xie , Jonathan J.D. McKendry , Johannes Herrnsdorf , *Member, IEEE*, Erdan Gu , Harald Haas , *Fellow, IEEE*, and Martin D. Dawson , *Fellow, IEEE*

Abstract—We report systematic investigation of the device-size-dependent performance of ultraviolet C (UV-C) light emitting diodes (LEDs) for optical wireless communication (OWC). Utilizing 273 nm-wavelength devices with diameters in the range of 40 μm to 300 μm , the size-dependent electrical, optical and frequency response characteristics of AlGaIn UV-C LEDs are analyzed. As the junction area scales down, the smaller devices present lower optical power but faster modulation speed. Based on a 1-m point-to-point OWC system, this study further explores the LED size effect on the communication performance including channel gain, signal-to-noise ratio (SNR), theoretical Shannon capacity, achievable data transmission rate, relevant ratio, and spectral efficiency (SE). The system employing a 60 μm diameter (micro) LED transmitter achieves the highest average SNR and SE accompanying a data transmission rate up to a 5.53 Gbps at the forward error correction floor of 3.8×10^{-3} . These results suggest an optimal device diameter of $\sim 60 \mu\text{m}$ for further development of high-performance UV-C short-range line-of-sight (LoS) OWC.

Index Terms—Optical wireless communications, size-dependent, UV-C LEDs.

I. INTRODUCTION

LIGHT emitting diodes (LEDs) based on the AlGaIn semiconductor alloy system have attracted considerable attention recently for operation across a significant portion ($\sim 200 \text{ nm} - 280 \text{ nm}$) of the ultraviolet C (UV-C) waveband. Such devices are applicable in various fields including water purification [1], sterilization [2], fluorescence microscopy [3], and optical communications [4]. These solid-state light sources are more environmentally friendly, robust, wavelength specific, have faster modulation speeds and lower costs compared with mercury lamps [5]. Notably, their fast modulation speeds have been a major driving force behind rapid technological advances

Manuscript received 7 September 2023; revised 18 October 2023; accepted 30 October 2023. Date of publication 3 November 2023; date of current version 16 November 2023. This work was supported in part by EPSRC under Grant EP/T00097X/1, and in part by Innovate UK under Grant 10005391. The work of Jordan Hill was supported by Fraunhofer U.K. Research Ltd. (*Jordan Hill and Cheng Chen contributed equally to this work.*) (*Corresponding author: Enyuan Xie.*)

Jordan Hill, Enyuan Xie, Jonathan J.D. McKendry, Johannes Herrnsdorf, Erdan Gu, and Martin D. Dawson are with the Department of Physics, Institute of Photonics, University of Strathclyde, G1 1RD Glasgow, U.K. (e-mail: jordan.hill@strath.ac.uk; Enyuan.Xie@strath.ac.uk; jonathan.mckendry@strath.ac.uk; johannes.herrnsdorf@strath.ac.uk; erdan.gu@strath.ac.uk; m.dawson@strath.ac.uk).

Cheng Chen and Harald Haas are with the LiFi Research and Development Centre, University of Strathclyde, G1 1RD Glasgow, U.K. (e-mail: c.chen@strath.ac.uk; harald.haas@strath.ac.uk).

Digital Object Identifier 10.1109/JPHOT.2023.3329980

in the field of optical communications, particularly for optical wireless communications (OWC) applications [6]. OWC is under widespread development as a complementary technology to the constrained and highly licenced radio frequency (RF) wireless communications [7]. The UV-based OWC offers several unique advantages over visible light communications for such applications, including a noise-free environment for outdoor communications due to the absorption of these wavelengths by the upper atmosphere. Additionally, this feature enables highly secure inter-satellite communication links that are invisible from ground level. Furthermore, UV light is highly scattered by the atmosphere due to Rayleigh and Mie scattering, which permits (where applicable) a non-line-of-sight mode of operation, relaxing line-of-sight (LoS) constraints on pointing and tracking transmitters and receivers [8]. Compared with the emissions within UV-A and UV-B bands, UV-C light possesses a shorter wavelength. It not only holds the promise of achieving higher data transmission rates, but also enhances the transmission range, signal-to-noise ratio (SNR) and security of UV-based OWC. Furthermore, recent research has affirmed that the emissions in the far-UV-C spectrum, specifically below a wavelength of 240 nm, exhibit relatively limited penetration depth, predominantly impacting the outer layers of the skin. Consequently, this diminishes the potential for deeper tissue damage and skin cancer risk in comparison to longer-wavelength of UV light. This distinctive attribute widens the range of potential applications for UV-C communication employing sub-240 nm light sources [9].

Several recent studies have explored the potential of OWC system employing UV-C LEDs as the transmitter, which include both conventional broad area LEDs (dimensions typically 300 $\mu\text{m} - 1 \text{ mm}$) and micro-LEDs (feature size below 100 μm). For example, Alkharzaji et al. demonstrated a 2.4 Gbps LoS link at a distance of 1 m using a 278 nm broad area LED [10]. By using a 262 nm micro-LED (active area equivalent to $\sim 27 \mu\text{m}$ diameter), He et al. in our group showed a 1.1 Gbps LoS link over a distance of 0.3 m [11]. Zhu et al. improved the micro-LED based OWC performance, reporting a 2 Gbps LoS link at 0.5 m using a 275 nm micro-LED [12]. Our recent research significantly improved upon the data transmission rate and transmission distances, showing a 6.5 Gbps UV-C micro-LED LoS link at a distance of 10 m and a 1 Gbps LoS link at a distance of 116 m [13]. These studies have highlighted the potential for UV-C based communication systems using a single LED as the transmitter. However, despite these promising results, there have only been limited investigations into the

lateral size effect (active area) of UV-C LEDs on the electrical and optical characteristics and on the overall performance of UV-C based OWC systems. Yu et al. highlighted size effects on the direct-current (DC) performance of UV-C LEDs, such as power and current densities [14]. However, further explorations of the size effect on the modulation characteristics and on the OWC performance are absent in their work. Recently, Qian et al. studied size-dependent behavior on data transmission rates as well as the spectral efficiencies (SE) in OWC systems, although the fabrication of the devices appears not to have been optimized, potentially masking the ideal trend data [15]. Given the imperative of determining the performance metrics involved, more comprehensive investigation is therefore necessary to fully comprehend these size effects and the impact they have on UV-C OWC systems.

Here we investigate the effect of lateral size on the DC and modulation characteristics of AlGaIn-based UV-C LEDs and their further application in short-range LoS OWC. High-performance UV-C LEDs with diameters in the range of $40\ \mu\text{m}$ to $300\ \mu\text{m}$, spanning the micro-LED to broad area LED regime, are demonstrated through an optimized fabrication process. Based on the measured DC and modulation characteristics of these UV-C LEDs, the pronounced size-dependent behaviors are revealed. A decrease in the lateral diameter of the LED results in an increase in both operation voltage and electrical modulation bandwidth, while a reduction in the light output power and external quantum efficiency (EQE) is observed. The impact of the lateral size on the communication performance is further explored through a 1-m point-to-point OWC system assuming a DC-biased optical-orthogonal frequency division multiplexing (DCO-OFDM) modulation scheme. The experimental setup utilized in this study represents the typical system for short-range LoS OWC, which offers numerous applications such as supporting on-chip level communication, serving as an optical interconnect for data centers and enhancing high-performance computing. The size-dependent behaviors of the channel gain, SNR, theoretical Shannon capacity, achievable data transmission rates, relevant ratio, and SE are investigated in detail. An optimal LED diameter of $60\ \mu\text{m}$, below which micro-LED performance begins to decline in channel gain, average SNR and SE, is determined for a high-performance short-range LoS DUV OWC system based on these results. The average SNR, data transmission rate and SE achieved by the $60\ \mu\text{m}$ micro-LED are, respectively, 1.19, 1.54 and 1.29 times higher than those of the broad area LED with $300\ \mu\text{m}$ diameter. On the other hand, when the device diameter is further reduced from $60\ \mu\text{m}$ to $40\ \mu\text{m}$, a sharp decline in the average SNR and SE is found, accompanied with a slight increase in the data transmission rate from 5.53 Gbps to 5.56 Gbps. The consequence of this study directly impacts the design and the fabrication of high-performance UV-C LEDs for future development of OWC applications.

II. DESIGN AND FABRICATION OF SIZE-DEPENDENT UV-C LEDs

The UV-C LED devices in a flip-chip configuration were fabricated from commercial-grade AlGaIn-based LED wafers

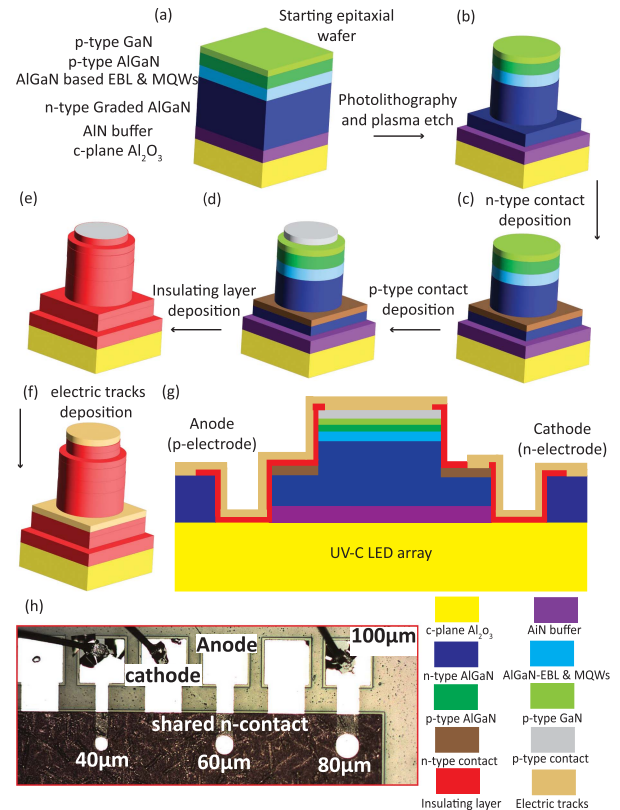


Fig. 1. (a)–(f) Simplified flip-chip UV-C LED fabrication process flow showing a single pixel through the fabrication steps and no bonding pad (vertical scale exaggerated), (g) cross-sectional schematic of the different-size UV-C LED, and (h) plan-view optical image of part of the fabricated size-dependent UV-C array.

grown 2” c-plane (0001) sapphire substrate. The wafer structure is similar to the one reported in our previous work, the details of which can be found in [11]. The detailed fabrication process of the through-substrate-emitting LEDs with different sizes are presented in Fig. 1(a)–(f). Standard UV photolithography and a chlorine-based inductively coupled plasma etching technique is used to define circular LED pixels of different diameters ranging from $40\ \mu\text{m}$ to $300\ \mu\text{m}$. After that, high-temperature annealed Ti/Al/Ti/Au and as-deposited Pd were employed as the ohmic contacts to n-type AlGaIn and p-type GaN, respectively. Then a SiO₂ passivation layer was deposited by plasma-enhanced chemical vapor deposition and the SiO₂ apertures on each mesa were subsequently created by plasma etching. Finally, Ti/Au tracks were deposited onto each pixel to simplify individual-anode addressing of each pixel with a shared cathode. A cross-section schematic of the fabricated UV-C LED is shown in Fig. 1(g). Compared with the devices reported in our earlier work [11], the one used here employed an optimized n-type metal contact to AlGaIn. The particular Ti/Al/Ti/Au metal scheme followed by high-temperature annealing guarantees an ohmic contact with a low specific contact resistivity and, in turn, better electrical performance for the UV-C LEDs as shown in the next section. The fabricated devices were wire-bonded to a printed circuit board without a heatsink installed for further characterization and OWC measurements. Fig. 1(h) shows a plain-view optical image of the exemplar UV-C LEDs with $40\ \mu\text{m}$, $60\ \mu\text{m}$, and $80\ \mu\text{m}$ diameters used in this work, the

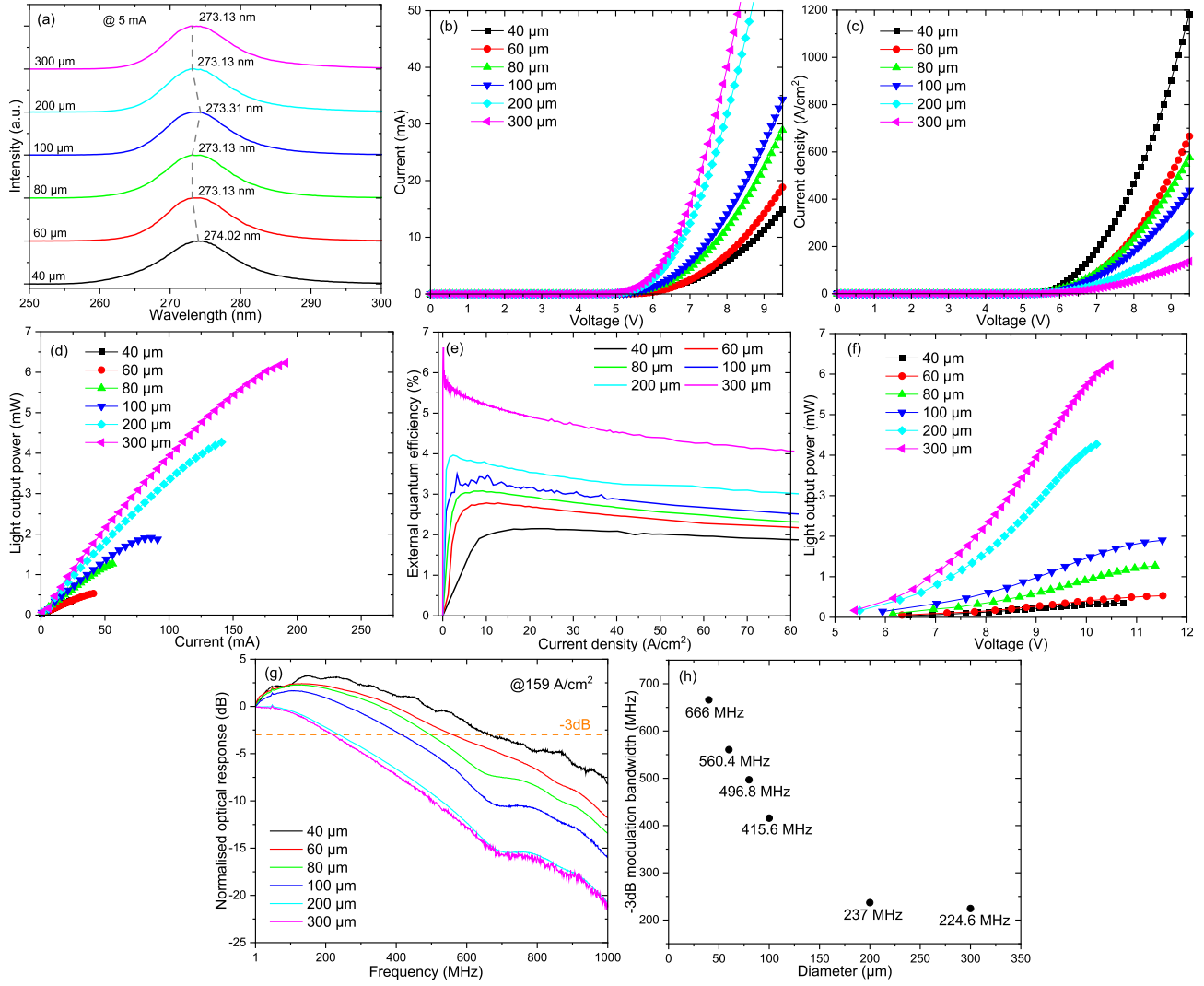


Fig. 2. (a) EL spectra at 5 mA, (b) I-V, (c) J-V, (d) L-I, (e) EQE vs J, (f) L-V, (g) normalised optical response of the fabricated UV-C LEDs with different diameters, orange dotted line representing -3 dB, and (h) maximum -3 dB modulation bandwidth versus device diameter at 159 A/cm². Due to the large scale and similar light output power between LEDs with 40 μ m and 60 μ m diameters, the corresponding data in part (d) overlap.

individual-addressable p-pads and shared n-pads are also included the image.

III. SIZE-DEPENDENT ELECTRICAL, OPTICAL AND FREQUENCY RESPONSE CHARACTERIZATION

Fig. 2(a) illustrates the electroluminescence (EL) spectra of different-size UV-C LEDs at an operation current of 5 mA. These spectra were measured by a spectrometer (Avantes, Avaspec-20482) with a fiber optic (Ocean optics, QP600-2-SR-BX). As shown, the different-size LEDs present similar emission peaks at around 273 nm with less than 1 nm variation. For different-size LEDs, the operation current (5 mA) corresponds to a wide operation current density range from a few A/cm² to hundreds of A/cm². Thus, these spectra not only prove the UV-C emission of our LEDs, but also demonstrate the peak stability of the devices under different bias levels.

Fig. 2(b), (c), and (d), respectively, present the current versus voltage (I-V), current density versus voltage (J-V), and light

output power versus current (L-I) characteristics of the fabricated UV-C LEDs with different diameters. The current density dependent characteristic is important to determine because of its importance to the modulation characteristics of the devices [16]. By placing a Si photodetector (Thorlabs, S120VC) in close proximity to the polished sapphire substrate (to directly measure the useful 'forward directed' light output power), these characteristics were measured at the same time using a current sweep on MATLAB using a DC power source (Yokogawa, GS610). As shown, these characteristics present a strong size-dependent behavior. As will be discussed, they depend upon a complex interplay of physical processes in the LEDs.

The electrical performance of the UV-C LEDs exhibits contrasting size-dependent trends, regarding the operation voltage in terms of current Fig. 2(b), and current density Fig. 2(c). The first observed size-dependent trend indicates that as the LED size gets smaller, the lower the operation current under the same bias voltage. As shown in Fig. 2(b), when the LEDs' diameters are reduced from 300 μ m to 40 μ m, the operation

voltages at 10 mA operation current of these different-sized devices increases from 6.65 V to 8.8 V. The trends depicted in Fig. 2(b) and (c) are the results of the change in LED junction area and also size-dependent changes in the parasitic series resistance. It is generally difficult to make precise estimates of the series resistance in UV-C LEDs due to their highly nonlinear I-V behavior. When estimating the series resistance by a linear fit, we observe an increase from 29.5 Ω to 158.7 Ω when the pixel diameter decreases from 300 μm to 40 μm , which is not a simple inverse proportional relationship with device area and is likely associated with improved current distribution in the n-AlGaIn layer in smaller LEDs. This size scaling of the series resistance is the reason that Fig. 2(c) shows the opposite trend compared to Fig. 2(b), i.e., a decrease in pixel diameter from 300 μm to 40 μm results in a decrease in operation voltage from 8.9 V to 6.52 V at an operation current density of 100 A/cm² (chosen as a current density achievable for all the devices across the full diameter range at a drive voltage <10 V). Smaller LEDs require lower operation currents than larger LEDs to achieve the same current density and, therefore, the voltage across the parasitic series resistance is less at a given current density. Here, it is important to indicate that, thanks to the optimized fabrication process developed in this work as well as availability of improved epitaxial structures, the electrical performance of the UV-C LEDs fabricated here presents a considerable improvement compared with devices reported in [11], [14], [15] and therefore exposes the ultimately limiting trends. This improvement not only results in a lower turn-on voltage, but also a larger maximum operation current and, in turn, higher achievable (forward directed) light output power as shown in Fig. 2(d). For all the LEDs, light output power increases continuously with increasing injection current until manually stopped before reaching thermal roll-over [17]. Larger LEDs can provide higher light output powers, due to the larger emission area and higher operation current that can be handled. The maximum (forward directed) light output power before roll-over varies from 0.5 mW to 6 mW with increased pixel size, which is consistently improved over values reported in the literature [11], [14], [15]. We want to emphasize that, it is important to indicate that, although the UV-C LEDs used in this study demonstrate the similar size effect on the electrical and optical characterizations with the one reported in other works [14], [15], their enhanced performance offers a wider dynamic range and better communication performance as presented in the next section. Fig. 2(e) illustrates the EQE versus J for the different-size UV-C LEDs. It is important to indicate that, the values shown in the figure should be below the actual values as only the forward directed light output power was recorded in our measurements. As shown, the peak EQE decreases from 6.62 % to 2.15 % when the devices diameter is reduced from 300 μm to 40 μm . On the other hand, the corresponded current density at peak EQE increases as the device diameter decreases, from 0.155 A/cm² for 300 μm LED to 24.3 A/cm² for 40 μm LED. Meanwhile, the efficiency droop behaviour is mitigated with device diameter decreasing. At 80 A/cm², the efficiency droop is reduced from 39 % in 300 μm LED to 16 % in 40 μm LED. These size-effect phenomena are similar with the ones observed in our early work [18].

In typical LED-based communication setups, the data is transmitted by applying a modulated voltage signal to the DC-biased LED. Therefore, the L-V characteristics of LEDs and in particular their linearity is important for the communication performance especially under the OFDM modulation scheme [19]. As shown in Fig. 2(f), the different size UV-C LEDs presents similar non linear behavior on the L-V characteristics. In the subsequent section we delve deeper into the impact of LED linearity on the performance of optical communications, exploring how the effect relates to the SNR. Another important aspect of the optical performance is the frequency response of the LEDs. To measure the frequency response of different-size UV-C LEDs, we utilized a small frequency-sweep modulation voltage generated by a network analyzer (Pico Technologies, PicoVNA 106), which was combined with a DC-bias current through a bias tee (Tektronix, PSPL5675 A). This combined signal was then applied to the LEDs. The optical response from LEDs was initially collected by UV-enhanced transceiver lens and subsequently focused by another UV-enhanced receiver lens onto a UV-enhanced avalanche photodiode (APD) detector (Hamamatsu, C5668 8867). It is important to note that, the APD detector used in this study features a wider frequency response range with a -3 dB bandwidth extending up to 1 GHz. This enhancement allows us to acquire more comprehensive and accurate frequency response data, overcoming the limitations observed in other works [11], [15]. Fig. 2(g) shows the frequency response measured across different-sized LEDs at the same current density of 159 A/cm² (chosen to be accessible by devices of all diameters). As shown, these responses follow a general trend that as the pixel diameter decreases the -3 dB electrical modulation bandwidth increases. The measured -3 dB electrical modulation bandwidth of these different-sized UV-C LEDs increases from 224.5 MHz to 666 MHz when the LED diameters decreased from 300 μm to 40 μm as highlighted in Fig. 2(h). A significant change in the modulation speed could be observed when the pixel diameter is below 100 μm . Limiting factors of the LED bandwidth are the resistance-capacitance (RC) time constant and the differential carrier recombination lifetime [11], [20]. Since these frequency responses were measured at the same current density with relatively low value, we attributed the observed increase in modulation bandwidth with reduced LED size to reduced RC time-constant and increased Shockley-Read-Hall recombination, the latter of which may be down to increased surface-to-volume ratio and therefore high defect density near the device perimeter. It is important to note that the -3 dB electrical modulation bandwidths achieved here for UV-C LEDs here are consistently higher than those reported in the literature for visible devices with similar LED dimensions [21]. This is mainly attributed to the comparatively higher density of defects present in AlGaIn-based UV-C LED wafers [22].

IV. OWC APPLICATION OF SIZE-DEPENDENT UV-C LEDs IN A POINT-TO-POINT SYSTEM

This section demonstrates and analyzes the size effect of the UV-C LEDs on the performance of a point-to-point OWC link. In the OWC measurement, the LEDs are employed as

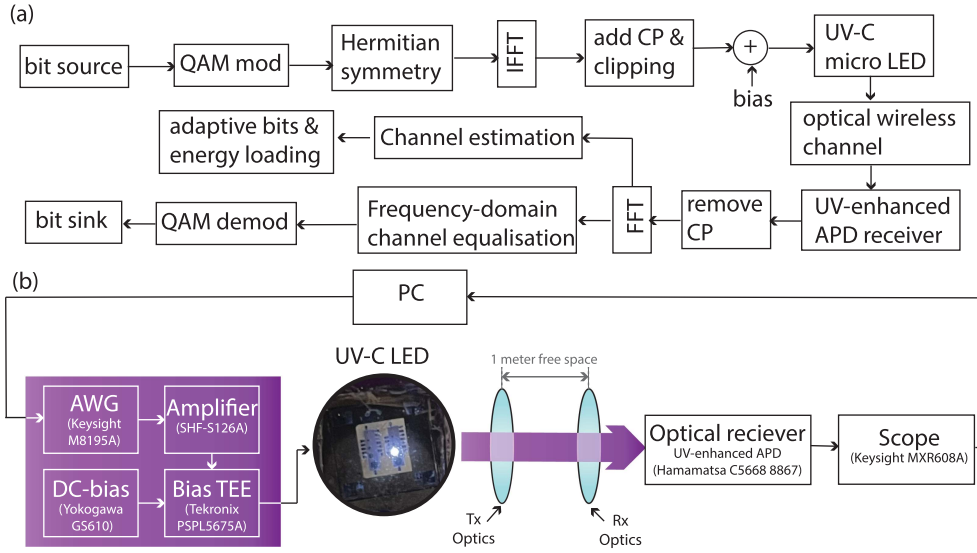


Fig. 3. (a) DCO-OFDM block diagram, and (b) Schematic diagram of the experimental setup for UV-C OWC measurements with an optical image of the UV-C LED with diameter of $300 \mu\text{m}$ in operation.

transmitters and a DCO-OFDM scheme is used for modulating and demodulating the data. DCO-OFDM is a widely used modulation scheme in optical communications systems and has been shown to be highly effective in maximizing the achievable data rate in channels with varying frequency. A block diagram of a DCO-OFDM system is illustrated in Fig. 3(a). On the transmitter side, binary information bits are modulated as quadrature amplitude modulation (QAM) symbols. To ensure a real-time-domain signal, a Hermitian symmetry operation is used. This will make $K/2-1$ out of K subcarriers carry information symbols, which $K = 2048$ is used in this study. Then, the frequency-domain QAM symbols are converted to time-domain OFDM symbols via a K -point inverse Fast Fourier Transform (IFFT) operation. To limit the OFDM signal peak-to-average power ratio (PAPR) and to ensure successful frequency-domain channel equalization, signal clipping and cyclic prefixes (CP) are added, respectively. The clipping level used in this work is 3.2 of the signal standard deviation and a CP length of 20 is found to be sufficient. On the receiver side, the detected signal is converted to a frequency domain signal by a Fast Fourier Transform (FFT) operation after the removal of CPs. With the help of pilot signals, the channel coefficient on each subcarrier can be accurately estimated. With the estimated channel information, the distorted symbols can be recovered with a single-tap equalization. In addition, the channel information can be used to estimate the SNR on each subcarrier and the transmitted energy and modulation depth can be adjusted accordingly. Eventually, the equalized QAM symbols are demodulated to binary bits [23], [24].

Shown in Fig. 3(b) below is a block diagram of the experimental setup used in this work. The OFDM waveforms are generated by MATLAB and forwarded to an arbitrary waveform generator (AWG) (Keysight, M8195 A) for digital-to-analog signal conversion. The output analog signals are then amplified by a high-power amplifier (SHF S126 A). Afterwards, the amplified signals and a DC-bias current were combined by a bias-T (Tektronix PSPL5575 A) and applied to the different-sized

UV-C LEDs. In order to achieve the highest data transmission rate, we have performed extensive experiments to determine the optimized DC-bias current and modulation depth V_{pp} for individual size UV-C LEDs, which are listed in Table I. The light emitted from the LEDs is firstly collimated by a 2-inch aspheric condenser lens with numerical aperture of 0.63 and $f/\# - 0.8$ (Tx optics: Edmund Optics, 84340). An equivalent lens (Rx optics) is employed to focus the light onto a UV-enhanced avalanche photo-diode (Hamamatsu, C5668 8867). The distance between two lenses is set at 1 m for all measurements to facilitate a comparison with other data. The output signals of the photodetector are captured by a digital oscilloscope (Keysight, DSA90804B) and sent back to the PC for decoding. The received optical power for each measurement are also measured by replacing the photoreceiver with a Si photodetector. As listed in Table I, the ratio between the transmitted and received optical power is around 70 % for all measurements. This indicates that similar collection efficiencies in the free-space link are achieved for all systems based on different-sized UV-C LEDs, which eliminates the possible influence from the optical setup on the communication performance.

A. Channel Gain

Firstly, the size effect on the channel gain of our UV-C LED-based OWC system was analyzed. Channel gain represents the amount of signal power received relative to the signal power transmitted from the LED. Fig. 4 illustrates the measured channel gain as a function of frequency achieved by the OWC system based on different-sized UV-C LED transmitters. As shown, a distinct size-dependent trend on the channel gain could be observed at low and high frequency regimes. Specifically, at low frequencies (<400 MHz), larger LEDs demonstrated higher channel gains than smaller LEDs, which may be attributed to their wider dynamic range and higher optical power. In the high frequency regime (>400 MHz), on the other hand, the

TABLE I
COMPARISON OF COMMUNICATION PERFORMANCE AND PARAMETERS FOR UV-C LEDs

Pixel diameter (μm)	40	60	80	100	200	300
Bias current density (A/cm^2) / current (mA)	955.4 / 12	566.2 / 16	477.7 / 24	458.6 / 36	194.3 / 61	107.6 / 76
V_{pp} at AWG (V)	0.12	0.12	0.13	0.15	0.19	0.27
-3 dB modulation bandwidth (MHz)	494	484	422	338	229	206
LOP at Tx/Rx (μW)	210 / 148	240 / 169	620 / 436	990 / 616	2160 / 1550	3090 / 2200
Average SNR (dB)	16.19	17.05	16.52	16.21	15.67	14.21
Shannon capacity (Gbps)	7.43	7.33	7.31	7.215	6.11	5.24
Achieved data rate ratio of channel capacity (%)	74.8	75.44	74	73	69.4	68.3
Spectral efficiency (bps/Hz)	3.67	3.72	3.60	3.50	3.06	2.89
Maximum constellation size	128	128	128	128	128	64

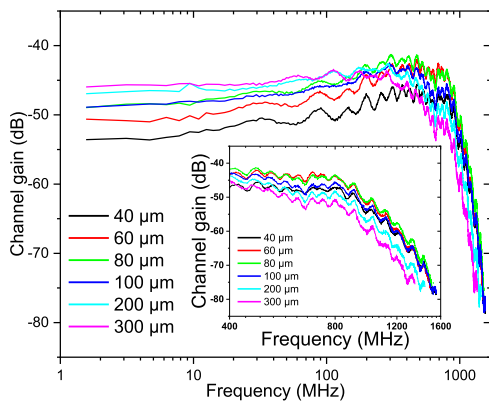


Fig. 4. Typical channel gains achieved by fabricated UV-C LEDs. Insert channel gains achieved at >400 MHz.

opposite trend was observed as smaller LEDs present higher channel gains than larger LEDs thanks to the benefit from the improved frequency response, which is highlighted as the insert of Fig. 4. On balance, the LED with $60 \mu\text{m}$ diameter presents the overall highest channel gain when considering a wide frequency band stretching beyond 400 MHz. It highlights that a diameter of $60 \mu\text{m}$ appears to be the optimal trade-off for UV-C based OWC for short-range LoS configuration. Here, it is also worth noting that although the $40 \mu\text{m}$ LED had the slowest roll off in the high frequency regime corresponding to the highest -3 dB modulation bandwidth in Table I, its channel gains are smaller than the other LEDs with diameters below $100 \mu\text{m}$. This observation indicates that, in the UV-C based OWC system, the low optical power produced from the smaller size LED leads to a degradation on the capability of link robustness. Its influence on data transmission rates will be further discussed in the following sub-section.

B. Signal-to-Noise Ratio

The size effect on the performance of the UV-C OWC systems using different-sized LED transmitters was also evaluated by analyzing the SNR versus frequency, as shown in Fig. 5(a). Generally, all-size LEDs achieve over 1 GHz bandwidth at SNR over 0 dB. This allows for a substantial number of parallel channels to be available for bit loading in the DCO-OFDM

format, approaching the limitation of data capacity. Moreover, improved SNR is observed for LED diameters below $100 \mu\text{m}$, and no significant difference in the SNR curves could be observed for the LED transmitters with diameters of $40 \mu\text{m}$, $60 \mu\text{m}$, $80 \mu\text{m}$, and $100 \mu\text{m}$. Here, it is important to point out that, in contrast to channel gain, the improvements in the SNR as the UV-C LED diameter decreases is observed across the whole frequency range including low frequencies. This indicates that the communication performance of larger UV-C LED transmitters does not benefit from their wider dynamic range and higher optical power even in the low frequency regime. In OWC systems, the SNR on each subcarrier is limited by receiver noise and nonlinear distortion. In order to explain the observed size-dependent behavior of SNR, the estimated SNR values across all LEDs solely deteriorated by receiver noise, in which identical training symbols are used on each subcarrier across all OFDM frames [17], are shown in Fig. 5(b). As shown, this trend presents a similar size-dependent behavior to that observed for the channel gains. Thus, it is reasonable to conclude that the nonlinear characteristics of different-sized UV-C LEDs plays a dominant role determining the size-dependent behaviors of SNR especially in the low frequency regime. This effect has been reported by Sun et al. [25] who state that nonlinear distortion is strongly dependent on the LED size. In order to further investigate the size effect on the SNR performance, the average SNRs of the OWC systems based on different-sized UV-C LED transmitters were calculated. The results are plotted in Fig. 5(c) and included in Table I. It was found that the average SNR keeps increasing as the LED diameter decreases to $60 \mu\text{m}$ but degrades when the LED diameter further reduces to $40 \mu\text{m}$. Compared with the LEDs of $300 \mu\text{m}$ and $40 \mu\text{m}$ diameters, the LED with an optimal diameter of $60 \mu\text{m}$ presents 1.20 and 1.05 times higher average SNR, respectively.

In addition to examining the average SNR, it is also important to determine the theoretical Shannon capacity for our DCO-OFDM modulation scheme. This provides a measure of the maximum achievable data rate in OWC systems using this modulation scheme. The theoretical Shannon capacity (C_{total}) can be calculated using the following formula [26]:

$$C_{\text{total}} = \sum_{i=1}^{\frac{K}{2}-1} \Delta B \log_2 \left(1 + \frac{S_i}{N_i} \right) \quad (1)$$

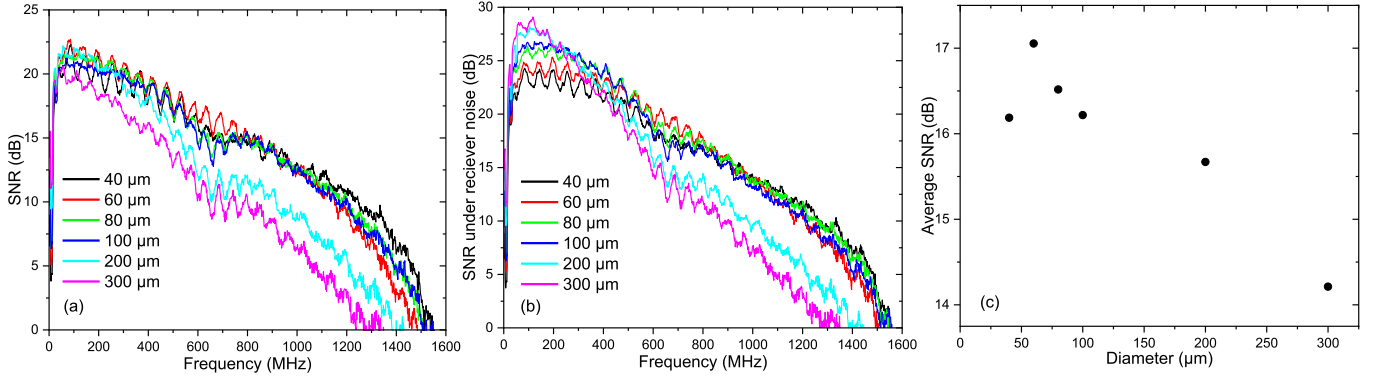


Fig. 5. (a) SNR versus frequency for the free-space point-to-point OWC experiment using the UV-C LEDs with a 1 m data transmission distance, (b) SNR under the sole effect of receiver noise versus frequency response for the same OWC experiment as shown in part (a), and (c) average SNR versus LED diameter.

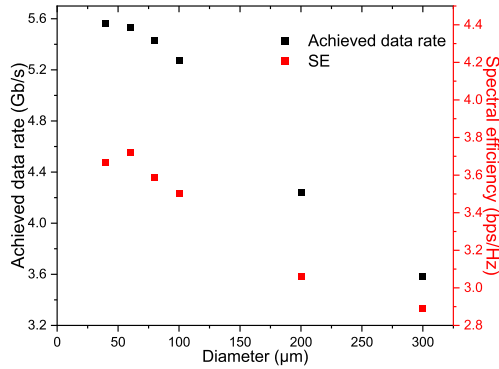


Fig. 6. Measured data transmission rates versus size at the FEC floor of 3.8×10^{-3} , and SE versus diameter, for the free-space point-to-point OWC experiment using UV-C LEDs with a 1 m data transmission distance.

Here, ΔB represents the available bandwidth for data transmission, S_i denotes the received signal power for integer values of i from 1 to $\frac{K}{2} - 1$, and N_i corresponds to the total channel noise power across the channel for integer values of i from 1 to $\frac{K}{2} - 1$, where K is the FFT size, and $\frac{K}{2} - 1$ is the number of information-carrying subcarriers. Thus, $\frac{S_i}{N_i}$ represents the SNR at different subcarriers as shown in Fig. 5(a). The calculated C_{total} based on the different-sized UV-C LED transmitters are detailed in Table I. Notably, the theoretical Shannon capacity shows greater enhancements when LED size is decreased below 100 μm. These findings supports the reduction of LED size yielding favourable enhancements in the optical communications performance.

C. Data Transmission Rate and Spectral Efficiency

Fig. 6 illustrates the measured data transmission rates at the forward error correction (FEC) floor of 3.8×10^{-3} and the corresponding SE for the UV-C OWC systems using different-sized LED transmitters. As shown, the data rate increases as the LED diameter is decreased. Up to 3.58 Gbps, 4.24 Gbps, 5.27 Gbps, 5.43 Gbps, 5.53 Gbps, and 5.56 Gbps data transmission rates were achieved for the UV-C LED transmitters with diameters of 300 μm, 200 μm, 100 μm, 80 μm, 60 μm, and 40 μm,

respectively. These achieved data transmission rates are considerably higher than those reported in e.g. [12], [15] using the similar size UV-C LED transmitters, which is mainly attributed to the improved electrical and optical performance of the LEDs fabricated using the optimized processing in this work. Compared with the 300 μm LEDs, over 50 % enhancement in data transmission rate is achieved when the device diameter is below 100 μm. However, this enhancement becomes less pronounced when the LED diameter decreases from 60 μm to 40 μm. Little difference in data transmission rate is found between the devices with 60 μm and 40 μm diameters. The achieved data rate ratio of channel capacity is illustrated in Table I, highlighting the relationship between the achieved data rate and the channel capacity. The UV-C LEDs follow a size-dependent trend with channel usage increasing from 68.3 % to 75.4 % with LED diameter decreasing from 300 μm to 60 μm, with a smaller drop off from 60 μm to 40 μm. These observations have implications for the size-dependent SE performances as illustrated in Fig. 6. As shown, the SE presents a clear decline when the LED diameter scales down from 60 μm to 40 μm. Similar to trends observed in channel gain and SNR, the diameter of 60 μm shows the best overall performance for short-range LoS OWC.

V. CONCLUSION

In this work, we systemically investigated the impact of device size on the electrical, optical, frequency response characteristics and further OWC applications of UV-C AlGaIn-based LEDs. Following an optimized fabrication process, high-performance 275 nm-wavelength LEDs with diameters in the range of 40 μm to 300 μm are demonstrated. As the LED diameter decreases, the smaller LEDs yield lower optical power but faster modulation speed and the exact size-dependence of the operational parameters is nonlinear. The influence of these size-dependent behaviors on the UV-C communication performance is further explored based on 1-m point-to-point OWC system assuming a DCO-OFDM scheme. Through analysis of the size-dependent characteristics on the typical short-range LoS OWC system including the channel gain, SNR, theoretical Shannon capacity, achievable data transmission rate and relevant ratio, and SE, we determine not only the dominant role of nonlinear features

from the different-size LEDs on communication performance, but also an optimal diameter of $60\ \mu\text{m}$ has pronounced enhancements in the average SNR, data transmission rate, and SE. Our finding offers valuable insights into the design and the fabrication of UV-C LEDs which paves the way towards further development of high-performance UV-C OWC systems.

REFERENCES

- [1] T. Matsumoto, I. Tatsuno, and T. Hasegawa, "Instantaneous water purification by deep ultraviolet light in water waveguide: Escherichia Coli bacteria disinfection," *Water*, vol. 11, no. 5, 2019, Art. no. 968.
- [2] H. Hirayama, S. Fujikawa, and N. Kamata, "Recent progress in AlGaIn-based deep-UV LEDs," *Electron. Commun. Jpn.*, vol. 98, no. 5, pp. 1–8, 2015.
- [3] T. Lu et al., "Rapid assessment of breast tumor margins using deep ultraviolet fluorescence scanning microscopy," *Proc. SPIE*, vol. 25, no. 12, 2020, Art. no. 126501.
- [4] P. Tian et al., "AlGaIn ultraviolet micro-LEDs," *IEEE J. Quantum Electron.*, vol. 58, no. 4, Aug. 2022, Art. no. 3300214.
- [5] Y. Muramoto, M. Kimura, and S. Nouda, "Development and future of ultraviolet light-emitting diodes: UV-LED will replace the UV lamp," *Semicond. Sci. Technol.*, vol. 29, no. 8, 2014, Art. no. 084004.
- [6] K. Kojima et al., "Self-organized micro-light-emitting diode structure for high-speed solar-blind optical wireless communications," *Appl. Phys. Lett.*, vol. 117, no. 3, 2020, Art. no. 031103.
- [7] H. Haas, "LiFi is a paradigm-shifting 5G technology," *Rev. Phys.*, vol. 3, pp. 26–31, 2018.
- [8] R. J. Drost and B. M. Sadler, "Survey of ultraviolet non-line-of-sight communications," *Semicond. Sci. Technol.*, vol. 29, no. 8, 2014, Art. no. 084006.
- [9] J. Nicholls et al., "High performance and high yield sub-240 nm AlN: GaN short period superlattice LEDs grown by MBE on 6 in. sapphire substrates," *Appl. Phys. Lett.*, vol. 123, no. 5, 2023, Art. no. 051105.
- [10] O. Alkhazragi et al., "Gbit/s ultraviolet-C diffuse-line-of-sight communication based on probabilistically shaped DMT and diversity reception," *Opt. Exp.*, vol. 28, no. 7, pp. 9111–9122, 2020.
- [11] X. He et al., "1 Gbps free-space deep-ultraviolet communications based on III-nitride micro-LEDs emitting at 262 nm," *Photon. Res.*, vol. 7, no. 7, pp. B41–B47, 2019.
- [12] S. Zhu et al., "2 Gbps free-space ultraviolet-C communication based on a high-bandwidth micro-LED achieved with pre-equalization," *Opt. Lett.*, vol. 46, no. 9, pp. 2147–2150, 2021.
- [13] D. M. Maclure et al., "Hundred-meter Gb/s deep ultraviolet wireless communications using AlGaIn micro-LEDs," *Opt. Exp.*, vol. 30, no. 26, pp. 46811–46821, 2022.
- [14] H. Yu et al., "AlGaIn-based deep ultraviolet micro-LED emitting at 275 nm," *Opt. Lett.*, vol. 46, no. 13, pp. 3271–3274, 2021.
- [15] Z. Qian et al., "Size-dependent UV-C communication performance of AlGaIn Micro-LEDs and LEDs," *J. Lightw. Technol.*, vol. 40, no. 22, pp. 7289–7296, Nov. 2022.
- [16] J. J. McKendry et al., "Visible-light communications using a CMOS-controlled micro-light-emitting-diode array," *J. Lightw. Technol.*, vol. 30, no. 1, pp. 61–67, Jan. 2012.
- [17] Z. Gong et al., "Size-dependent light output, spectral shift, and self-heating of 400 nm InGaIn light-emitting diodes," *J. Appl. Phys.*, vol. 107, no. 1, 2010, Art. no. 013103.
- [18] P. Tian et al., "Size-dependent efficiency and efficiency droop of blue InGaIn micro-light emitting diodes," *Appl. Phys. Lett.*, vol. 101, no. 23, 2012, Art. no. 231110.
- [19] D. A. Tsonev, "High speed energy efficient incoherent optical wireless communications," Ph.D. dissertation, Sch. Eng., Univ. Edinburgh, Edinburgh, U.K., 2015.
- [20] R. P. Green, J. J. McKendry, D. Massoubre, E. Gu, M. D. Dawson, and A. E. Kelly, "Modulation bandwidth studies of recombination processes in blue and green InGaIn quantum well micro-light-emitting diodes," *Appl. Phys. Lett.*, vol. 102, no. 9, 2013, Art. no. 091103.
- [21] J. Zhao et al., "GaIn-based parallel micro-light-emitting diode arrays with dual-wavelength $\text{In}_x\text{Ga}_{1-x}\text{N}/\text{GaIn}$ MQWs for visible light communication," *Opt. Exp.*, vol. 30, no. 11, pp. 18461–18470, 2022.
- [22] M. Shatalov et al., "AlGaIn deep-ultraviolet light-emitting diodes with external quantum efficiency above 10%," *Appl. Phys. Exp.*, vol. 5, no. 8, 2012, Art. no. 082101.
- [23] D. Tsonev et al., "A3-Gb/s single-LED OFDM-based wireless VLC link using a gallium nitride μLED ," *IEEE Photon. Technol. Lett.*, vol. 26, no. 7, pp. 637–640, Apr. 2014.
- [24] M. S. Islim et al., "Towards 10 Gb/s orthogonal frequency division multiplexing-based visible light communication using a GaIn violet micro-LED," *Photon. Res.*, vol. 5, no. 2, pp. A35–A43, 2017.
- [25] Z. Sun et al., "A power-type single GaIn-based blue LED with improved linearity for 3 Gb/s free-space VLC without pre-equalization," *IEEE Photon. J.*, vol. 8, no. 3, Jun. 2016, Art. no. 7904308.
- [26] M. Parker, "Error-correction coding," *Digit. Signal Process.*, vol. 101, 1986, Art. no. 146.